Multi-sensor array for polarimetric light-field imaging

Yunsong Nie[a], Chongde Zi[*b], Yunqian Li[b], Tao Yue[b], Xun Cao[b]
[a]Beijing institute of space mechanics & electricity, Beijing, China; [b]School of electronic science and engineering, Nanjing University, Nanjing, China

ABSTRACT

Both light-field and polarization information contain lots of clues about scenes, and they can be widely used in variety of computer vision tasks. However, existing imaging systems cannot simultaneously capture the light-field and polarization information. In this paper, we present a low-cost and high-performance miniaturized polarimetric light-field camera, which is based on the six heterogeneous sensors array. The main challenge for the proposed strategy is to align the multi-view images with different polarization characteristics, especially for regions with high degree of polarization -- in which the intensity correlations are commonly weak. To solve this problem, we propose to use Convolutional Neural Network (CNN) based stereo matching method for aligning the heterogeneously polarized images accurately. After stereo matching, both the light field and the Stokes vectors of scene are estimated, and the polarimetry conventions, e.g., the polarization angle, the linear polarization degree and the circular polarization degree, are given. We implement the prototype of the multi-sensor polarization light-field camera and perform extensive experiments on it. The polarimetric light-field camera achieves six live streaming on time and the heterogeneous processor of NVIDIA Jetson TX2 is exploited for image processing. Benefiting from the multi-sensor parallel polarization imaging and efficient parallel processing, the proposed system achieves promising performance on time resolution, signal-to-noise ratio. Besides, we develop the object recognition applications to show the superiorities of proposed system.

Keywords: polarimetric imaging, multi-sensor, light-field, convolutional neural network, Stokes parameters, image registration

1 INTRODUCTION

Polarized information from the natural scenes carries lots of valuable clues that are often ignored by common cameras or imaging systems. However, it can play a significant role in numerous fields, such as chemistry, geology, astronomy and so on[1,2]. Traditional polarization photography is mainly used in remote sensing, optical researches and military fields, while in recent decades it begins to be applied to people's daily lives, such as 3D films and display technologies[3,4,5]. In order to extend the applications of the polarization camera system to solve the computer vision and computational photography tasks, including target detection, image enhancement, 3D shape reconstruction etc., we introduce the multi-sensor array for polarimetric light-field imaging[6,7].

Indeed, polarization can be represented in a variety of mathematical methods, such as basic trigonometric function representation, Jones vector[8], Stokes parameters[9], graphic method and so on, among which the Stokes parametric method is most widely used because of its characteristic of simple measurement. Thus, in this paper, we apply the Stokes parametric method to generate the polarization information from multi-view scenes captured by the camera. In order to measure the Stokes parameters, there are usually three options, i.e. the modulation method[10], the rotation method[11] and the micro-polarizer array[12,13]. The second system usually can be altered from common cameras by adding a linear polarizer in front of it, so multiple images with different polarization directions can be acquired through rotating the polarizer or camera. As to the micro-polarizer array, it is similar to the principle of Bayer sensor in that there are different organized polarizers mounted on top of adjacent pixels, so we can directly generate the polarization information from the sensor. It can be seen from the implementations of these camera systems that the polarizer rotating method sacrifice the time dimension for imaging thus is difficult to obtain a high framerate and also the measurement accuracy of the camera system is greatly affected by the mechanical structure. Though the micro-polarizer array overcomes these defects, it relies on the manufacturing process more that inevitably increases the cost.

*zichongde@smail.nju.edu.cn

Another problem of the proposed system is the multi-sensor images registration without which we cannot derive the Stokes parameters from the 6 heterogeneous sensors. The purpose here is to find the accurate correspondence between each 2 of them. Inspired by the work of Yang et. al[14], we apply the similar registration method based on depth information, which is feasible since the convolutional neural network (CNN) based stereo matching algorithm can extract feature vectors more accurately than traditional stereo methods without the need of intensity fidelity difference.

In all, we propose to use the Stokes parametric method to measure the polarization information of the scene captured by the multi-sensor camera array. According to the Stokes parameters, we can derive and classify both the polarized and non-polarized images of the real scenes to analyze the polarization states. We also introduce the implementation details of our prototype multi-sensor array camera and problems of light field reconstruction, convolutional neural network (CNN) based multi-view image registration and the deviation correction. Finally, we evaluate the performance of the system through experiments and discuss its application prospects.

2 METHODOLOGY

Most sources of light are classified as incoherent and unpolarized (or only "partially polarized") because they consist of a random mixture of waves having different spatial characteristics, frequencies (wavelengths), phases, and polarization states. However, with the help of superposition principle, we consider that a wave with any specific spatial structure is a mixture of plane waves which is easy to deal with mathematically. More specifically, the complex polarization light can be decomposed into a linear superposition of multiple purely polarized lights[15]. Given that linear polarization and circular polarization can be seen as special cases of elliptical polarization, a polarization state can be described in relation to the geometrical parameters of the ellipse and its “handness”.

It is easy to understand if we discuss the polarization ellipse from the perspective of electromagnetic waves. Suppose that a plane electromagnetic wave with a frequency of ω propagates along a certain direction and we define its propagation direction as the axis z, then its components on axis x and y are represented as[16]:

$$\begin{cases} E_x = a_1 \cos(\tau + \delta_1) \\ E_y = a_2 \cos(\tau + \delta_2) \end{cases} \tag{1}$$

Here $\tau = \omega t - \boldsymbol{k} \cdot \boldsymbol{r}$ represents the variable part of the phase factor, $\boldsymbol{k}$ represent wave vector, $\boldsymbol{r}$ is the location vector of the space point, and a_1, a_2 represents the magnitude of E_x, E_y respectively. If we define $\delta = \delta_2 - \delta_1$ and eliminate the time-dependent factor τ, we can obtain the parametric equations of E_x and E_y with respect to δ:

$$\left(\frac{E_x}{a_1}\right)^2 + \left(\frac{E_y}{a_2}\right)^2 - 2\frac{E_x}{a_1}\frac{E_y}{a_2}\cos(\delta) = \sin^2(\delta) \tag{2}$$

The equation above corresponds to an elliptic equation, which can be used to describe linear and circular polarizations under certain conditions. Stokes proposed a method for characterizing ellipse polarization, i.e. Stokes parameters, which is able to describe the states of lights mixed with both purely polarized and unpolarized components. There are 4 parameters for plane monochromatic waves in Stokes method that can be represented as:

$$\boldsymbol{S} = \begin{bmatrix} s_0 \\ s_1 \\ s_2 \\ s_3 \end{bmatrix} = \begin{bmatrix} a_1^2 + a_2^2 \\ a_1^2 - a_2^2 \\ 2a_1 a_2 \cos\delta \\ 2a_1 a_2 \sin\delta \end{bmatrix} \tag{3}$$

where $\boldsymbol{S}$ represents the Stokes vector. We can also deduce the relationship between the elliptically polarized orientation angle ψ and ellipticity angle χ from these parameters.

$$\begin{cases} s_1 = s_0 \cos 2\chi \cos 2\psi \\ s_2 = s_0 \cos 2\chi \sin 2\psi \\ s_3 = s_0 \sin 2\chi \end{cases} \tag{4}$$

The orientation angle ψ, the ellipticity angle χ and the Stokes parameters $\boldsymbol{S}$ can be plotted directly in a 3-D Poincaré sphere. Thus, it is obvious that Stokes parameters have great convenience in describing the states of elliptically polarized light, including pure and hybrid polarization states.

Another convenient aspect about Stokes method is that we can compute the polarization states of incident light indirectly through the measurement of intensity in different cases. For example, it is feasible to use 4 heterogeneous direction linear polarizers, i.e. $\theta = \{0, \pi/4, \pi/2, 3\pi/4\}$ and a quarter-wave plate with phase delay $\beta = \pi/4$ to measure the Stokes parameters following the equations below[17]:

$$\begin{cases} s_0 = I(0,0) + I(\pi/2,0) \\ s_1 = I(0,0) - I(\pi/2,0) \\ s_2 = I(\pi/4,0) - I(3\pi/4,0) \\ s_3 = I(\pi/4,\pi/2) - I(3\pi/4,\pi/2) \end{cases} \tag{5}$$

where $I(\theta,\beta)$ represent the intensity obtained directly from the corresponding sensor when the angle of linear polarizer is θ and the phase delay is β.

3 SYSTEM

3.1 System configuration

As shown in Figure 1 we implement the prototype of the multi-sensor polarization light-field camera, that is a combination of 6 different polarizers, 6 CMOS sensors and 1 embedded processing platform. Specifically, the 6 polarizers of 12.5mm diameter we used including 4 linear polarizers (polarization directions are 0°, 45°, 90° and 135° respectively) and 2 circular polarizers (left-handed and right-handed) are from Edmund Optics[18], which feature about 42% transmission of visible light from 400 to 700 nm. As to the sensors, we use 6 Raspberry Pi Camera[19] with 800 million pixels resolution, 3.04mm focal length and 73.8° field of view (FOV). The data captured by the sensors is synchronously transmitted to the NIVIDIA Jetson TX2 processing board for image processing through the adapter circuit board that we designed. The whole camera system is stable and flexible, which enables us to move them freely in experiments.

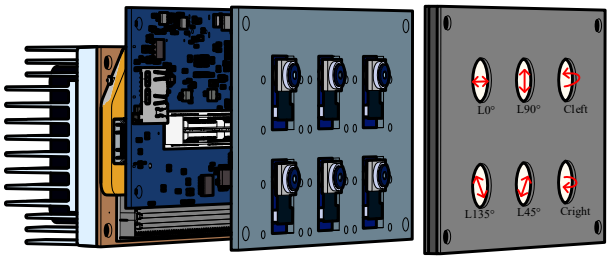

(c) (b) (a)

Figure 1. The prototype of the multi-sensor polarization light-field camera. (a) Six different polarizers, (b) Six CMOS sensors array, (c) The Jetson TX2 embedded processing platform.

3.2 Processing flow

After the configuration of the multi-sensor array, TX2 is exploited for image capturing and processing. First of all, we obtain the raw polarization data from the real scenes. Then we calibrate the system in order to apply the CNN based stereo matching algorithms[20], since the rectification need to be applied before matching to correct the system errors. Once we have computed the disparity maps of multi-view images, we can warp them to any reference image plane for registration and the error rate can be decreased using the proposed deviation correction method. Finally, the Stokes parameters are computed to extract both the polarized and unpolarized images of the scene, which can also be utilized to analyze the polarization states and applied to practical applications. The whole processing flow is demonstrated in Figure 2 below and the implementation details will be discussed in Section 4.

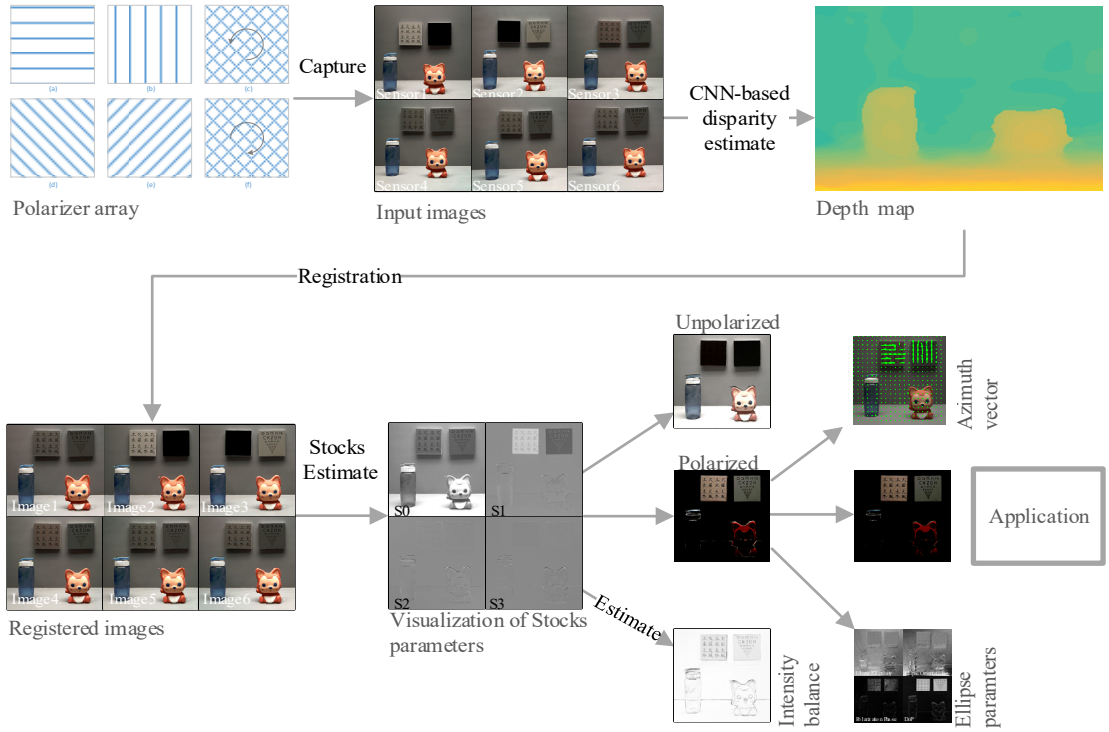

Figure 2. The whole processing flow of our multi-sensor camera.

4 IMPLEMENTATION

4.1 Camera calibration and stereo rectification

Each sensor is mounted by one specific polarizer that have different polarization angles respectively. Since the intensity difference of the flat chessboard patterns captured directly by the 6 sensors is not too obvious in the natural scene, the classic camera calibration technique proposed by Zhang[21] is still applicable here. Given the intrinsic parameters and distortion coefficients, we can compute the undistorted images of 6 sensors.

Then we do stereo calibration for 6 sensors, which is necessary since we will need to acquire stereo rectification image pairs for solving stereo matching problem later. However, there is no need to calculate all of the 15 possible pairs since we can choose the reference image plane to simplify the problem. Specifically, we apply the same rectification algorithm in OpenCV on 2 horizontal rows (both with the rightmost camera as reference) and the rightmost column (with the up left camera as reference) to avoid computing the image pairs both in different columns and rows in which case the epipolar lines are neither horizontal or vertical.

4.2 CNN-based stereo matching and disparity map prediction

In fact, after the modulation by different polarizes, lenses and sensors, the same object point of 3-D coordinates from the scene will project 6 different image points of 2-D coordinates on heterogeneous image planes. The intensity difference between image patches caused by 6 polarizers in different orientations will definitely influence the accuracy of stereo matching as well. The main task here is to find the accurate correspondence between each 2 of them and acquire the registration results, which can be used to compute the polarization information of the scene. Thus, a convolutional neural network (CNN) based stereo matching algorithm is used to extract the disparity map for solving the problem, since the Convolutional Neural Network mimics the human eye neurons well and can extract feature vectors more accurately than traditional stereo methods without the need of intensity fidelity difference.

We briefly introduce the networks here to make the paper self-complete. The fast architecture is a siamese work, i.e. two shared-weight sub-networks joined at the head. The sub-networks are composed of a number of convolutional layers with

rectified linear units following all but the last layer. As to the accurate architecture, it is derived from the former by replacing the cosine similarity with a number of fully connected layers, which increased the running time but decreased the error rate. The raw outputs of the network still have some errors, especially in low-texture regions and occluded areas. Thus, a series of post-processing steps, i.e., cross-based cost aggregation, semi-global matching, a left-right consistency check, subpixel enhancement, a median, and a bilateral filter, are applied to refine the quality of raw disparity maps.

Indeed, we apply both the fast and slow pre-trained networks of Middlebury and KITTI stereo data sets on our real captured images to achieve better disparity maps, thus we can extract light field information through the calibrated parameters of our camera model.

4.3 Multi-sensor images registration

Theoretically, by applying the stereo rectification and matching on all image pairs, we can derive disparity maps between all of them, thus to warp to any image plane of the 6 sensors. In fact, there is no need to warp all images to all the views. In experiment, we choose the up left sensor as our destination. As to the two images at different rows and different columns, instead of computing the stereo matching directly, we warp one of them through the intermediary images which are at the same row of one input image and at the same column with the other. Thus, by applying the stereo rectification and matching on 2 horizontal rows (both with the rightmost camera as reference) and the rightmost column (with the up left camera as reference), we can obtain all of the 6 registration images on the same image plane. Note that all the registration images are undistorted, which means any rectified images pairs need to be remapped to the ideal image plane of the chosen reference sensor, i.e. the inverse process of stereo rectification by setting the distortion coefficients to null.

4.4 Stokes parameters estimation

Based on the camera configuration and multi-sensor images registration, it is feasible to apply the Stokes parametric method to decompose both the polarized and non-polarized information from the scene, since Stokes matrix can describe not only the purely polarization states, but also the states of unpolarized and partially polarized light. The model we use to extract the original Stokes vectors can be expressed as:

$$\begin{bmatrix} s_0 \\ s_1 \\ s_2 \\ s_3 \end{bmatrix} = \boldsymbol{A} \cdot \boldsymbol{I} = \begin{bmatrix} 1 & 0 & 1 & 0 & 0 & 0 \\ 1 & 0 & -1 & 0 & 0 & 0 \\ 0 & 1 & 0 & -1 & 0 & 0 \\ 0 & 0 & 0 & 0 & 1 & -1 \end{bmatrix} \cdot \begin{bmatrix} I(0,0) \\ I(\pi/4,0) \\ I(\pi/2,0) \\ I(3\pi/4,0) \\ I(\pi/4,\pi/2) \\ I(3\pi/4,\pi/2) \end{bmatrix} \tag{6}$$

where $s_i(i = 0,1,2,3)$ represents each component of the Stokes vector, $\boldsymbol{A}$ is the constant modulation matrix, $\boldsymbol{I}$ is the intensity acquired from the sensor. Suppose that the total intensity captured by the sensor is s_0, we formulate it as a superposition of the polarized and unpolarized light (i.e. s_p and s_{unp}):

$$s_0 = s_p + s_{unp} \tag{7}$$

According to the Stokes method, s_p can be computed as:

$$s_p = \sqrt{{S_1}^2 + {S_2}^2 + {S_3}^2} \tag{8}$$

Then we can decompose both of the polarized and unpolarized component from the total intensity, i.e.:

$$\begin{cases} \mathbf{S_p} = [s_p \quad s_1 \quad s_2 \quad s_3]^H \\ \mathbf{S_{unp}} = [s_0 - s_p \quad 0 \quad 0 \quad 0]^H \end{cases} \tag{9}$$

Where H means the transposition operation of matrices. With the Stokes parameters, we can analyze the polarization states from some aspects including the degree of polarization(*DOP*), the degree of linear polarization(*DOLP*), the degree of circular polarization(*DOCP*), the ellipse eccentricity χ and orientation angle ψ. They can be calculated as followed:

$$DOP = \frac{s_p}{s_0},\ DOLP = \frac{\sqrt{{S_1}^2+{S_2}^2}}{s_0},\ DOCP = \frac{s_3}{s_0} \tag{10}$$

$$\chi = \frac{1}{2}\sin^{-1}\left(\frac{S_3}{s_p}\right),\ \psi = \frac{1}{2}\tan^{-1}\left(\frac{S_2}{S_1}\right) \tag{11}$$

where $\sin^{-1}$ and $\tan^{-1}$ respectively represent the inverse sine and tangent function. After the unpolarized light is separated from the polarized light, the circularly polarized light is removed and purely linear polarized light is obtained.

$$\begin{bmatrix} I_{lpx} \\ I_{lpy} \\ I_{lpa} \\ I_{lpb} \end{bmatrix} = \begin{bmatrix} I(0,0) \\ I(\pi/4,0) \\ I(\pi/2,0) \\ I(3\pi/4,0) \end{bmatrix} - \frac{s_{unp}}{2}\begin{bmatrix} 1 \\ 1 \\ 1 \\ 1 \end{bmatrix} - s_3\begin{bmatrix} 1 \\ 1 \\ 1 \\ 1 \end{bmatrix} \tag{12}$$

where I_{lpx}, I_{lpy}, I_{lpa}, I_{lpb} respectively represent the intensity captured by the 4 sensors which mounted with linear polarizers in different angles, i.e. $0, \pi/4, \pi/2, 3\pi/4$. However, the extracted value of linear polarized light is always positive which loses the polarization direction information. In order to solve the problem, we introduce a quadrant discriminative method to tell the difference of linear polarized light with the same intensity. The model is demonstrated in the following Table 1:

Table 1. The quadrant discriminative method based on the characteristics of intensity.

Characteristics of intensity	Linear polarization angle range
$I_{lpx} \geq I_{lpy}$ $I_{lpa} > I_{lpb}$	$(0, \pi/4]$
$I_{lpx} < I_{lpy}$ $I_{lpa} \geq I_{lpb}$	$(\pi/4, \pi/2]$
$I_{lpx} \leq I_{lpy}$ $I_{lpa} < I_{lpb}$	$(\pi/2, 3\pi/4]$
$I_{lpx} > I_{lpy}$ $I_{lpa} \leq I_{lpb}$	$(3\pi/4, \pi]$

According to the table, we utilize the relationship between $\left(I_{lpa}, I_{lpb}\right)$ to classify the angles of linear polarization into 4 categories, and thus restore the direction of I_{lpx}:

$$lpx = \begin{cases} lpx, & I_{lpa} \geq I_{lpb} \\ -lpx, & I_{lpa} < I_{lpb} \end{cases} \tag{13}$$

We can also compute the original azimuth angle φ of the linear polarized light by:

$$\varphi = \cos^{-1}\left(\frac{\sqrt{I_{lpy}}}{\sqrt{I_{lpx}+I_{lpy}}}\right) \tag{14}$$

where $\cos^{-1}$ is the inverse cosine function.

5 EXPERIMENTS

5.1 Experimental system construction

We implement the multi-sensor array as shown in Figure 3, which mainly consist of three components including the 6 polarizers mounted on the surface, 6 heterogeneous sensors array and the TX2 processing platform. The whole camera system is stable and portable, which is convenient to be put into practical applications. Following the steps demonstrated in Figure 2, we do experiments on sorts of real captured scenes to evaluate and verify the feasibility and efficiency of our prototype camera as well as the proposed polarimetric light-field reconstruction method.

Figure 3. The multi-sensor array for polarimetric light-field imaging.

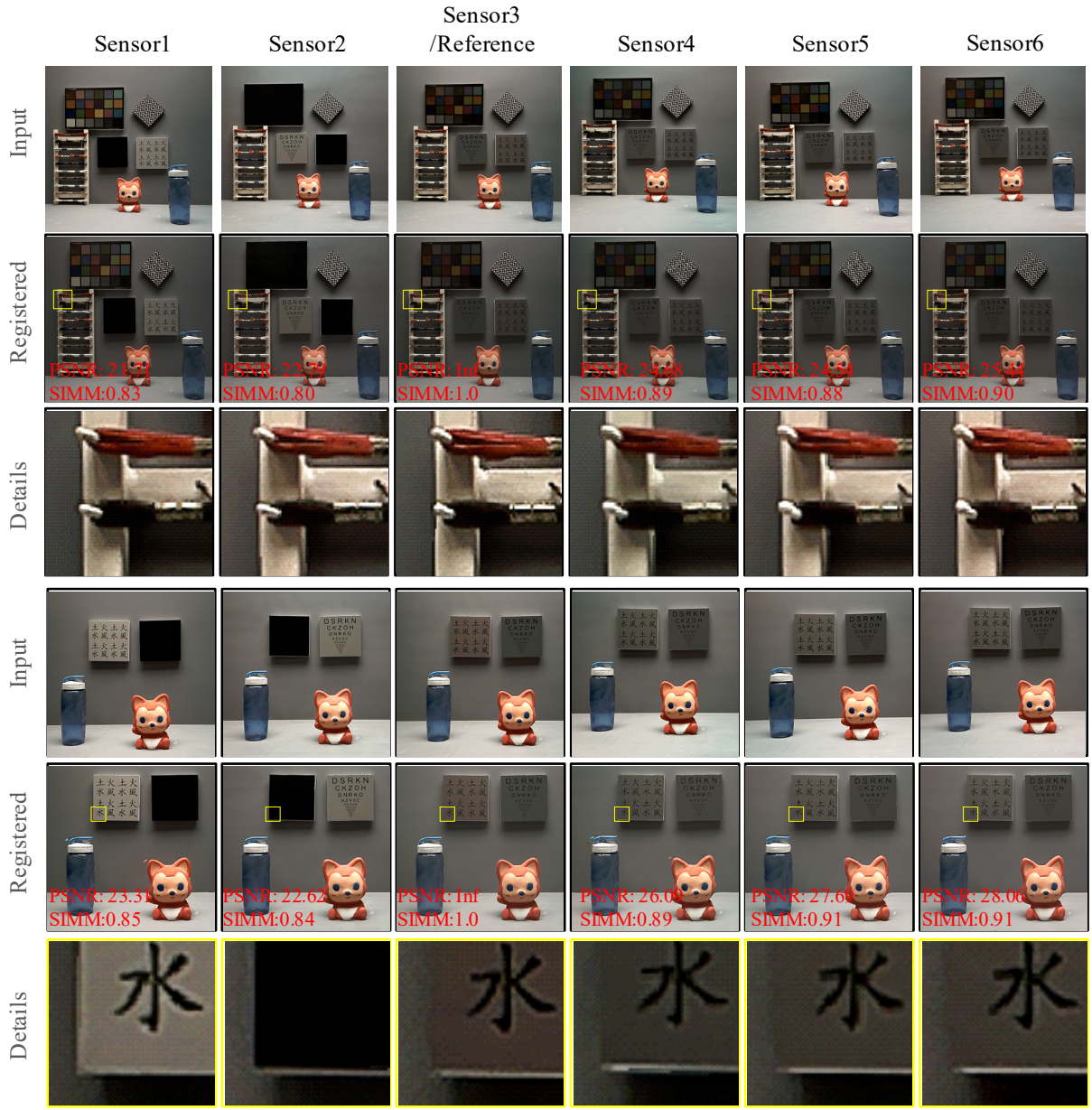

Figure 4. Contrast between the input images and registration images with details illustrated.

5.2 CNN based alignment

In order to test the robustness of the CNN based stereo matching algorithm, we construct various well-designed scenes. For example, we use multiple linear polarizers with different polarization angles to cover the objects in the scene randomly, which results in the intensity difference of multi-view sensors. Without the need of intensity fidelity difference, the stereo matching accuracy can meet our requirements both effectively and efficiently.

Figure 4 demonstrates the experiment results on two natural scenes captured in our laboratory with the PSNR and SSIM between the reference image and each of the others. More intuitively, the selected details are illustrated to show the precision of the registration method. Note that any sensor could be chosen to be the reference, because the proposed method makes no restrictions on that and is flexible to be applied in practice.

5.3 Reconstruct polarization information

Then we decompose both the polarized and unpolarized information from the original scene via the measurement of Stokes parameters as shown in Figure 2. After the visualization of Stokes parameters, something interesting is observable, e.g. the distribution sensitivity of the elliptical polarization angle on the reflective surface, as shown in Figure 5.

As to the three horizontally placed board, it is obvious that we can distinguish them from the rest of the objects in the decomposed polarized and unpolarized images, i.e. image (b) and (c), while it will be a challenging mission for the mixture light image, i.e. image (a). Meanwhile, in order to verify the computation accuracy of the multi-sensor array for polarimetric light field imaging, we also derive the image of ellipse orientation angle, which is sensitive to the direction of reflection, and the image of ellipse polarization phase. The deviation correction of registration is applied here to suppress the error rate.

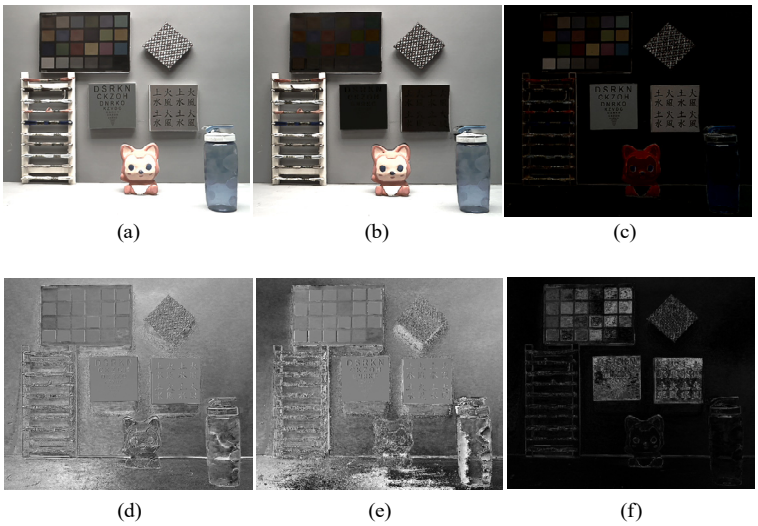

Figure 5. Polarization information reconstruction. (a) Mixed light image, (b) Unpolarized light image, (c) Polarized light image, (d) Ellipse eccentricity image, (e) Ellipse orientation angle image, (f) Ellipse polarization phase image.

5.4 Evaluation of the azimuth measurement

We characterize the degree and angle of linear polarization. As shown in Figure 6(a), we select a smooth region in the image and calculate the distribution of the linear polarized angle measurement results. There are more than 900 points in the selected area of interest. The average result is about 91.05 degrees, and the standard deviation is 0.21degrees.

Besides, we evaluate the linearity of the camera by using an electronically controlled rotary table with high precision of 0.00625 degrees. The linear polarizer is installed on the electronically rotary table. We set the rotation step to 10 degrees at a time and finish the measurement when the polarizer rotates 180 degrees. Figure 6(b) shows the instrument and results of the test. From the fitting result, i.e. SSE(Sum squared error): 31.9922, RSQUARE(Coefficient of determination): 0.9993, RMSE(Root mean squared error):1.4140, we can see that the multi-sensor camera has a good characteristic of linearity.

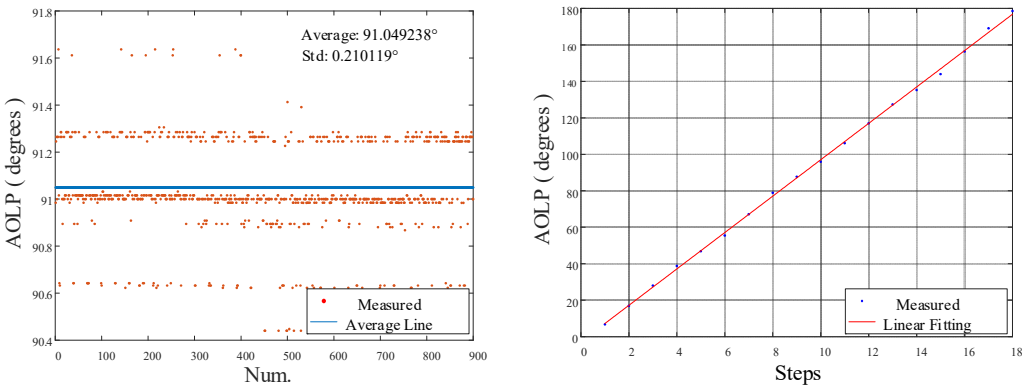

(a) (b)

Figure 6. Evaluation of measurement error and linearity. (a) Error distribution in region of interest. (b)The electronically controlled rotary table mounted with a linear polarizer and the linear fitting result(Linear model: Azimuth(num) = 9.977*num - 2.78; SSE: 31.9922; RSQUARE: 0.9993; RMSE:1.4140).

5.5 Preliminary application

According to the demonstrated experiments above, we have proved the feasibility and efficiency of our proposed multi-sensor array system. As to preliminary application, we follow the similar processing steps discussed in this paper and manage to decode the hidden polarization information from the scene. Figure 7 below intuitively demonstrates the interesting processing of decoding the "password" of the environment. We create a test pattern using a number of polarizing blocks with the same shape and color but different directions. The general camera cannot identify the text above the chart (Figure 7(a)), but it is easy for our camera to detect it, i.e. the "SPIE" character on the chart, enhanced and shown in Figure 7 (d).

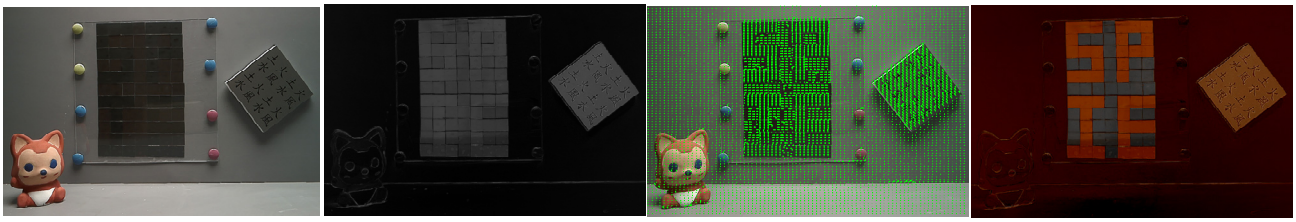

(a) (b) (c) (d)

Figure 7. Preliminary application example. (a) Image captured by normal camera which is not sensitive to polarization, (b) Degree of polarization (DOP) image, (c) Linear polarization azimuth image, (d). Synthesis image from DOP and azimuth.

6 CONCLUSION

In this paper, we present a multi-sensor array camera for polarimetric light-field imaging. The prototype camera is a combination of 6 different polarizers, 6 CMOS sensors and 1 embedded processing platform. The data captured by the sensors is synchronously transmitted to the NIVIDIA Jetson TX2 processing board for image processing. By applying the CNN based stereo matching algorithm, we register the heterogeneous polarization images efficiently. Thus, the Stokes parameters are estimated to extract both polarized and unpolarized information of the scene, which could also be utilized to analyze the polarization states and applied to practical applications.

The prototype camera is both stable and flexible, which is convenient to carry on developments and researches. However, there is still a lot of work need to be invested in, such as multi-sensor intensity response calibration, the polarizers construction error, the accuracy of robust depth prediction algorithm etc. The practical prospects of the system can be extended to apply in more complex tasks in computer vision and many other fields.

ACKNOWLEDGEMENTS

This work was supported by Grant No. 61671236 and No. 61627804 from National Natural Science Foundation of China, Grant No. BK20160634 from National Natural Science Foundation for Young Scholar of Jiangsu Province, and Grant No. 0210-14380067 from Fundamental Research Funds for the Central Universities, China.

REFERENCE

[1] Adamson, A., Aspin, C., Davis, C., & Fujiyoshi, T., "Astronomical polarimetry: current status and future directions, " Astronomical Society of the Pacific Conference Series 343, 15-19 (2005).
[2] Snik, F., Keller, C., “Astronomical polarimetry,” in Planets, Stars and Stellar Systems, 7 (2012).
[3] Scott Tyo J., Goldstein Dennis L., Chenault David B., and Shaw Joseph A., "Review of passive imaging polarimetry for remote sensing applications", Applied Optics 45(22), 5453-5469 (2006).
[4] Larive, M., Collot, L., Breugnot, S., Botma, H., & Roos, P. "Laid and flush-buried mines detection using 8-12 mu m polarimetric imager, " Proceedings of SPIE - The International Society for Optical Engineering, 3392 (1998).
[5] Morel, O., Stolz, C., Meriaudeau, F., & Gorria, P. "Active lighting applied to three-dimensional reconstruction of specular metallic surfaces by polarization imaging," Appl Opt 45(17), 4062-4068 (2006).
[6] Nicolas, L., Nicolas, L., Sebastien B., Philippe C., "Compact and robust linear Stokes polarization camera," Proc. SPIE 6972, 7 (2008).
[7] Cong, P. H., Robles-Kelly, A., & Hancock, E. R., "Shape and refractive index recovery from single-view spectro-polarimetric images," International Journal of Computer Vision, 101(1), 64-94 (2013).
[8] Jones, R. C., “A new calculus for the treatment of optical systemsiii. the sohncke theory of optical activity,” Josa, 31(6), 500-503(1941).
[9] Mcmaster, W. H., "Polarization and the stokes parameters, "s American Journal of Physics 22(22), 351-362 (1954).
[10] William S., Thomas A. Germer, John W. Mac K., and Frans S., "Compact and robust method for full Stokes Spectropolarimetry," Applied Optics 51(22), 5495-5511 (2012).
[11] Kadambi, A., Taamazyan, V., Shi, B., & Raskar, R., "Polarized 3D: High-Quality Depth Sensing with Polarization Cues," IEEE International Conference on Computer Vision, 3370-3378 (2016).
[12] Nordin, G. P., Meier, J. T., Deguzman, P. C., & Jones, M. W., "Micropolarizer array for infrared imaging polarimetry, " Journal of the Optical Society of America 16(5), 1168-1174 (1999).
[13] Kikuta, H., Numata, K., Muto, M., Iwata, K., Toyota, H., & Moriwaki, K., et al., "Polarization imaging camera with a form birefringent micro-retarder array," Frontiers in Optics, (2003).
[14] Yang, Z., Yue, T., Linsen, C., Hongyuan, W., Zhan, M., et al. "Heterogeneous camera array for multispectral light field imaging," Optics Express 25(13), 14008 (2017).
[15] Goldstein D., [Polarized Light, 3rd], CRC Press, New York, 10-18(2011).
[16] Born M, Wolf E. [Principles of Optics, 7rd ed.], Cambridge University Press, Cambridge, 12-15(2001).
[17] Collett, A. E., [Field Guide to Polarization], SPIE Press, Washington, 5-20 (2005).
[18] Edmund Optics, "12.5mm Diameter Unmounted, Linear Glass Polarizing Filter," Edmund Optics Website, 2018, <https://www.edmundoptics.com/optics/polarizers/linear-polarizers/12.5mm-diameter-unmounted-linear-glass-polarizing-filter/> (2018).
[19] Raspberry Pi Foundation, "Camera Module V2 - Raspberry Pi," Raspberry Pi Website, 1 April 2016, <https://www.raspberrypi.org/products/camera-module-v2/> (2018).
[20] Lecun, Y., "Stereo matching by training a convolutional neural network to compare image patches," JMLR.org 17 (1), 2287-2318 (2016).
[21] Zhang, Z., "A flexible new technique for camera calibration," Tpami 22(11), 1330-1334 (2000).